



CELL DEATH

Alternative splicing of *GSDMB* modulates killer lymphocyte-triggered pyroptosis

Qing Kong^{1+*}, Shiyu Xia^{2,3†}, Xingxin Pan⁴, Kaixiong Ye^{5,6}, Zhouyihan Li¹, Haoyan Li¹, Xiaoqiang Tang¹, Nidhi Sahni^{7,8}, S. Stephen Yi^{4,9,10}, Xing Liu¹¹, Hao Wu^{12,13}, Michael B. Elowitz^{2,3}, Judy Lieberman^{12,14}, Zhibin Zhang^{1*}

Copyright © 2023 The Authors. Some rights reserved; exclusive licensee American Association for the Advancement of Science. No claim to original U.S. Government Works

Granzyme A from killer lymphocytes cleaves gasdermin B (*GSDMB*) and triggers pyroptosis in targeted human tumor cells, eliciting antitumor immunity. However, *GSDMB* has a controversial role in pyroptosis and has been linked to both anti- and protumor functions. Here, we found that *GSDMB* splicing variants are functionally distinct. Cleaved N-terminal (NT) fragments of *GSDMB* isoforms 3 and 4 caused pyroptosis, but isoforms 1, 2, and 5 did not. The nonfunctional isoforms have a deleted or modified exon 6 and therefore lack a stable belt motif. The belt likely contributes to the insertion of oligomeric *GSDMB*-NTs into the membrane. Consistently, noncytotoxic *GSDMB*-NTs blocked pyroptosis caused by cytotoxic *GSDMB*-NTs in a dominant-negative manner. Upon natural killer (NK) cell attack, *GSDMB*3-expressing cells died by pyroptosis, whereas *GSDMB*4-expressing cells died by mixed pyroptosis and apoptosis, and *GSDMB*1/2-expressing cells died only by apoptosis. *GSDMB*4 partially resisted NK cell-triggered cleavage, suggesting that only *GSDMB*3 is fully functional. *GSDMB*1-3 were the most abundant isoforms in the tested tumor cell lines and were similarly induced by interferon- γ and the chemotherapy drug methotrexate. Expression of cytotoxic *GSDMB*3/4 isoforms, but not *GSDMB*1/2 isoforms that are frequently up-regulated in tumors, was associated with better outcomes in bladder and cervical cancers, suggesting that *GSDMB*3/4-mediated pyroptosis was protective in those tumors. Our study indicates that tumors may block and evade killer cell-triggered pyroptosis by generating noncytotoxic *GSDMB* isoforms. Therefore, therapeutics that favor the production of cytotoxic *GSDMB* isoforms by alternative splicing may improve antitumor immunity.

INTRODUCTION

Pyroptosis, a lytic form of programmed necrotic cell death that releases inflammatory mediators to activate immune responses, is mediated by pore-forming gasdermins (*GSDMs*). The human *GSDM* family consists of five active members: *GSDMA*, *GSDMB*, *GSDMC*, *GSDMD*, and *GSDME* (1). After the C-terminal (CT) autoinhibitory domains are removed by proteolysis, the N-terminal (NT) domains of these *GSDMs* bind lipids, oligomerize, and form pores in the plasma membrane to induce pyroptosis (2–9).

Granzyme B (GzmB) from killer lymphocytes causes cancer-associated pyroptosis (CAP) by cleaving *GSDME* in tumor cells (10). CAP increases immune cell infiltration into the tumor and elicits antitumor protection (11, 12). Similarly, killer cell granzyme A (GzmA) cleaves *GSDMB* to trigger CAP (13). *GSDMB* expression, which can be induced by tumor necrosis factor- α or interferon- γ (IFN- γ), markedly increases the efficacy of immune checkpoint blockade in mouse tumor models (13).

Nevertheless, the role of *GSDMB* in CAP is controversial. The pore-forming activity of *GSDMB*-NT was verified in some studies (13, 14) but disputed in others (15–17). The concept that *GSDMB* triggers CAP and antitumor immunity has also been challenged in studies showing that *GSDMB* expression in gastric and breast cancers correlates with poor clinical outcomes (18–20) and that *GSDMB* promotes cell proliferation and migration during epithelial repair in a pyroptosis-independent manner (15). Five *GSDMB* isoforms are generated by alternative splicing of exons 6 and 7, leading to different *GSDMB*-NTs upon cleavage by GzmA. Most of the previous studies focused on one isoform without considering that distinct isoforms might have different functions. Here, we investigate the functions of *GSDMB* splicing variants and find that only isoforms 3 and 4, which contain an intact exon 6, trigger killer cell-mediated pyroptosis. Our study systematically defines the functional landscape of *GSDMB* isoforms and reveals a role of alternative splicing in modulating CAP.

¹Department of Immunology, University of Texas MD Anderson Cancer Center, Houston, TX 77054, USA. ²Division of Biology and Biological Engineering, California Institute of Technology, Pasadena, CA 91125, USA. ³Howard Hughes Medical Institute, California Institute of Technology, Pasadena, CA 91125, USA. ⁴Livestrong Cancer Institutes, Department of Oncology, Dell Medical School, University of Texas at Austin, Austin, TX 78712, USA. ⁵Department of Genetics, Franklin College of Arts and Sciences, University of Georgia, Athens, GA 30602, USA. ⁶Institute of Bioinformatics, University of Georgia, Athens, GA 30602, USA. ⁷Department of Epigenetics and Molecular Carcinogenesis and Department of Bioinformatics and Computational Biology, University of Texas MD Anderson Cancer Center, Houston, TX 77030, USA. ⁸Quantitative and Computational Biosciences Program, Baylor College of Medicine, Houston, TX 77030, USA. ⁹Interdisciplinary Life Sciences Graduate Programs (ILSGP) and Department of Biomedical Engineering, University of Texas at Austin, Austin, TX 78712, USA. ¹⁰Oden Institute for Computational Engineering and Sciences (ICES), University of Texas at Austin, Austin, TX 78712, USA. ¹¹Center for Microbes, Development and Health, Key Laboratory of Molecular Virology and Immunology, Institut Pasteur of Shanghai, Chinese Academy of Sciences, Shanghai, 200031, China. ¹²Program in Cellular and Molecular Medicine, Boston Children's Hospital, Boston, MA 02115, USA. ¹³Department of Biological Chemistry and Molecular Pharmacology, Harvard Medical School, Boston, MA 02115, USA. ¹⁴Department of Pediatrics, Harvard Medical School, Boston, MA 02115, USA.

*Corresponding author. Email: qkong1@mdanderson.org (Q.K.); z Zhang16@mdanderson.org (Z.Z.)

†These authors contributed equally to this work

RESULTS**GSDMB isoforms differ in pore-forming activity**

The conflicting GSDMB literature prompted us to investigate whether GSDMB isoforms exhibit different pore-forming activities. GSDMB isoforms are generated by alternative splicing of exons 6 and 7. According to previous studies (13, 21), we designated the five previously reported isoforms as gasdermin B1 (exon 6 skipping, $\Delta 6$; 403 amino acids), B2 ($\Delta 6, \Delta 7$; 394 amino acids), B3 (416 amino acids, no exon skipping), B4 ($\Delta 7$; 407 amino acids), and B5 ($\Delta 7$ and a 12-nucleotide insertion in exon 6 due to an alternative splicing acceptor; 411 amino acids) (Fig. 1A). In addition, in this study, we identified a new isoform that we named GSDMB6.

The original study identifying the GzmA-GSDMB pathway examined GSDMB3 (13), whereas two recent studies, which found no pore-forming activity, tested GSDMB5 (15, 17). To determine whether GSDMB-NTs, generated by GzmA cleavage of different GSDMB isoforms (fig. S1), exhibit pore-forming activity, we ectopically expressed the NTs of GSDMB1-5 in human embryonic kidney (HEK) 293T cells. As previously reported, GSDMD-NT and GSDME-NT induced pyroptosis (2, 3, 22, 23), whereas only the GSDMB3- and B4-NTs caused pyroptosis, as indicated by cell membrane ballooning (Fig. 1, B and C) and lactate dehydrogenase (LDH) release (Fig. 1D). The other GSDMB isoforms were noncytotoxic although the NT fragments were well expressed, indicated by immunoblotting (Fig. 1E). Cytotoxic NT fragments of GSDMB3 and GSDMB4 were barely detected because of cell death. Full-length (FL) GSDMB has been shown to bind membrane lipids (24). To test whether FL GSDMBs also induce pyroptosis, we expressed FL GSDMB1-5 isoforms in HEK293T cells (Fig. 1I). None of them were cytotoxic, as indicated by normal cell morphology (Fig. 1, F and G) and background LDH release (Fig. 1H). GzmA was shown to cleave GSDMB3 at two sites, a major site, K244, and a minor site, K229 (fig. S1), generating a long (GSDMB3-NT244) and a short NT (GSDMB3-NT229), respectively (13). Only the long GSDMB3-NT244, but not the short cleavage fragment GSDMB3-NT229, induced pyroptosis when ectopically expressed in HEK293T cells (Fig. 1, B to E).

GSDMB-NT has also been shown to bind to bacterial membranes and kill bacteria (17). To test whether GSDMB-NTs kill bacteria, NTs of GSDMB1-5 were ectopically expressed in BL21 *Escherichia coli* through isopropyl- β -D-thiogalactopyranoside (IPTG) induction. Only GSDMB3-NT244 and GSDMB4-NT killed bacteria (Fig. 1, J and K), whereas the other isoforms were noncytotoxic, although the NT fragments were well expressed, as indicated by immunoblotting (Fig. 1L). Thus, GzmA only generates GSDMB pores when it cuts GSDMB3 at the major cleavage site and GSDMB4, but not the other isoforms, reconciling the seemingly conflicting observations in the literature.

A belt motif in GSDM-NT promotes pore formation

To investigate why GSDMB isoforms have contrasting pore-forming activities, we compared the predicted structural models of GSDMB-NT isoforms generated by AlphaFold (25) with structures of human GSDMD-NT and mouse GSDMA3-NT obtained by cryo-electron microscopy (cryo-EM) and x-ray crystallography (5, 9, 26–28). Previous truncation experiments identified residues 1 to 243 as the minimal GSDMD-NT fragment capable of inducing pyroptosis (2, 29). Further scanning mutagenesis demonstrated

that Thr²³⁹ and Phe²⁴⁰ are necessary for GSDMD-NT activity (29). Thr²³⁹ and Phe²⁴⁰ in GSDMD, and the corresponding residues in GSDMA3 (Thr²³¹ and Phe²³²), are visible in both membrane-inserted and autoinhibited conformations (Fig. 2, A to C) (5, 9, 26, 27). In these structures, the $\beta 9$ and $\beta 11$ strands form a hairpin that is stabilized by a belt motif that wraps around the hairpin and ends with the critical Thr and Phe residues just near the GSDM-NT C terminus. The ThrPhe residues nest inside a cavity formed by the $\alpha 3$ - $\beta 6$ - $\beta 9$ region by forming hydrogen bonding and hydrophobic interactions (Fig. 2C) (9, 29). Therefore, the belt is not part of the disordered linker between the NT and CT domains of GSDMs but rather is an ordered, integral structure within the active NT domain. Cryo-EM structures of the membrane-inserted GSDMB (30, 31) published during the revision of this manuscript confirmed the orderedness of the belt.

The GSDMB-NT splicing variants only differ in their sequences in the belt motif (Fig. 2A). In GSDMB-NT, the critical Thr in the ThrPhe residues is replaced by a conservative Ser \rightarrow Thr substitution. The noncytotoxic NTs of GSDMB isoforms 1 and 2 and the short form of 3 (3S; NT229) all lack the critical SerPhe residues (Fig. 2A). The sequences of the pore-forming GSDMB4-NT and long form of GSDMB3-NT (3L; NT244) are identical in this region, whereas GSDMB5 has a four-residue insertion, potentially disrupting the belt and shifting residues within the belt (Fig. 2A), in line with a recent cryo-EM analysis of GSDMB5 (30). Structural modeling of GSDMB-NT isoforms indicated that the belt is unstable in isoforms 1, 2, 3S (NT229), and 5, which either lack the $\beta 9$ - $\beta 11$ hairpin, have the C terminus hanging far from the $\alpha 3$ - $\beta 6$ - $\beta 9$ cavity because of the lack of SerPhe, or both (Fig. 2D). Consistently, crystal structures of GSDMB5 showed that the belt is disordered in this isoform (30–32). Therefore, the belt motif in isoforms 3L and 4, which resembles the stabilizing structures formed in GSDMD and GSDMA3, is necessary for pore formation and unstable in the noncytotoxic isoforms.

Noncytotoxic GSDMB-NTs are incapable of membrane insertion

To examine the mechanism by which the belt motif promotes the pore-forming activity of GSDMB-NTs, we first investigated whether GSDMB-NTs differ in lipid binding. There are positively charged residues within the variable belt region (Fig. 2A). According to predicted structures, the positively charged residues (R225, K227, and K229) in GSDMB3-NT244 and GSDMB4-NT are clustered and point toward the membrane. The unstable belts in the NTs of GSDMB1, GSDMB2, GSDMB3S, and GSDMB5 alter the positions and orientations of the positively charged residues, potentially hindering lipid binding by these isoforms (Fig. 2E). However, when we incubated purified GSDMB-NTs with strips dotted with different lipids, all GSDMB-NTs similarly bound to cardiolipin, PtdIns(4)P [phosphatidylinositol 4-phosphate], and phosphatidylserine, suggesting that the belt motif does not markedly influence lipid binding of GSDMB-NTs (Fig. 2F). It is possible that there are subtle lipid binding differences under the detection limit of our assay, because triple charge-reversal mutations of R225-K227-K229 modestly lowered the activity of GSDMB3 in liposome-based experiments (30). Nonetheless, less-aggressive double mutations of R225-K227 to alanines did not affect GSDMB3 activity (31), supporting our postulation that the belt promotes pore formation mainly by an alternative mechanism. Besides the lipid strip

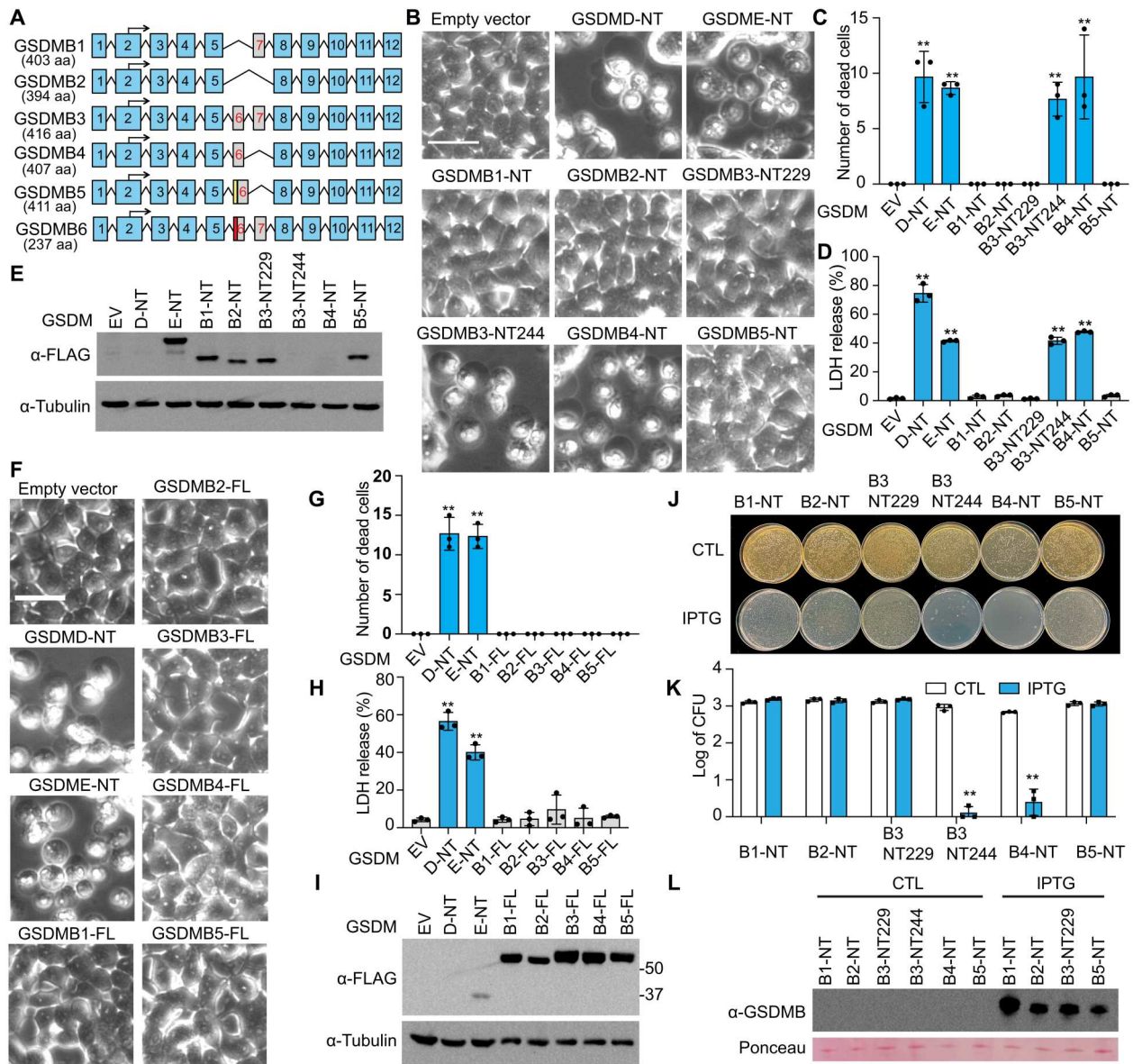


Fig. 1. NT fragments of GSDMB splicing isoforms exhibit different pore-forming activity. (A) Schematic of six alternative splicing variants of GSDMB. Numbered blue boxes represent exons. An alternative splicing acceptor results in an insertion (yellow box) in exon 6 of GSDMB5. The red box in GSDMB6 indicates a 13-nucleotide deletion in exon 6. (B to E) The effect of overexpressing GSDMB-NTs on HEK293T cell death, assessed by morphology using microscopy (B and C) and by LDH release (D). Dead cells were counted and quantified using three images (C). Expression of indicated FLAG-tagged GSDMB-NTs was determined by anti-FLAG immunoblot (E). (F to I) The effects of overexpressing FL GSDMBs on HEK293T cell death, assessed by morphology using microscopy (F and G) and by LDH release (H). Dead cells were counted and quantified using three images (C). Expression of indicated FLAG-tagged FL GSDMBs was assessed by anti-FLAG immunoblots (I). (J to L) The effect of overexpressing NT GSDMBs on *E. coli* cell death, assessed by colony formation on LB plates without (CTL; nontreatment) or with IPTG (J and K). CFU, colony-forming units. Expression of indicated NT GSDMBs was assessed by anti-GSDMB immunoblots (L). Ponceau S-stained bands were used as loading controls. Data are mean \pm SD of biological triplicates and are representative of three independent experiments. Statistical analysis was performed using the two-tailed Student's *t* test. $**P < 0.01$. Scale bars, 20 μ m.

results, all GSDMB-NTs contain the hydrophobic anchor and three positively charged patches previously identified as crucial for membrane binding by GSDM-NTs (9, 26, 32). In addition, the positively charged residues within the GSDMB belt are not conserved among GSDMs (Fig. 2A).

Next, we tested whether GSDMB-NTs differ in oligomerization, because the belt is located near an intersubunit contact site (9, 26).

We expressed NT fragments or FL GSDMB splicing isoforms in HEK293T cells and analyzed the lysates by immunoblotting in denaturing or native gels (Fig. 2G). Under denaturing conditions, all proteins migrated mostly as monomers. Under native conditions, high-molecular weight oligomers were visible in cells transfected with GSDMB-NTs but not GSDMB-FLs. Oligomers were barely detectable for cytotoxic GSDMB3-NT244 and GSDMB4-NT because

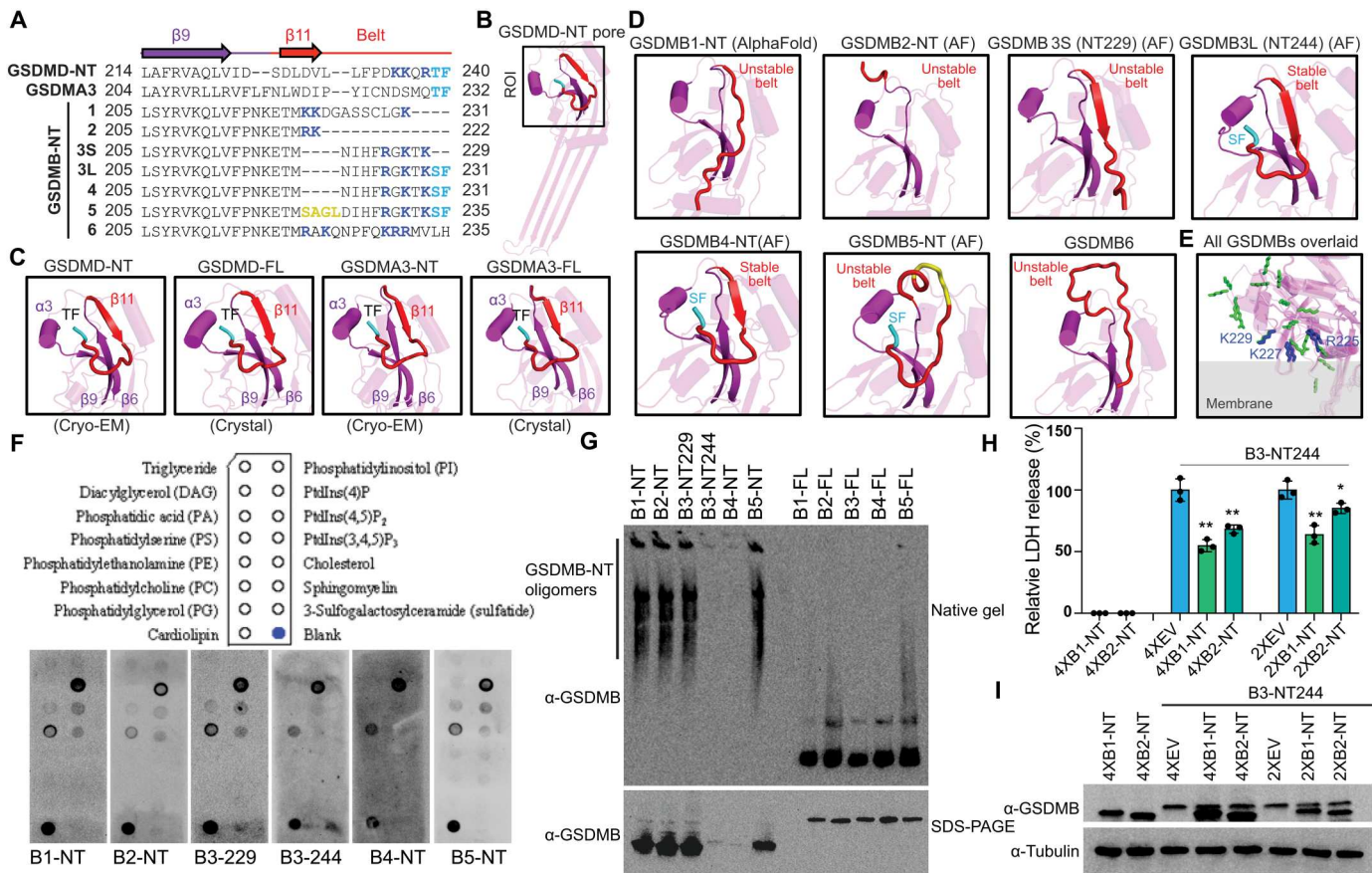


Fig. 2. Structural and functional analysis of NT GSDMB isoforms. (A) Sequence alignment of the NT domains (NTs) of human GSDMD, mouse GSDMA3, and human GSDMB variants near the belt motif (red). Arrows: β strands. Yellow: Extra residues in the belt in GSDMB5. Blue: Positively charged residues in the belt. Cyan: ThePhe or SerPhe residues necessary for GSDMD-NT activity. Dashes: Missing residues. (B) Cryo-EM structure of the human GSDMD-NT pore [Protein Data Bank (PDB): 6VFE] showing a single subunit. The region of interest (ROI), near the belt, is boxed and enlarged in (C). (C) Zoomed-in views of the belt regions of GSDMD and GSDMA3 in both membrane-inserted (cryo-EM structures; PDB: 6VFE and 6CB8) and autoinhibited (crystal structures; PDB: 6N9O and 5B5R) conformations. For clarity, residues after the belt, including the linker and GSDM-CTs, are not shown. 3S, GSDMB3-NT229; 3L, GSDMB3-NT244. (D) AlphaFold structural models of the GSDMB-NT variants, zoomed-in at the belt region (red). For clarity, residues after the belt are hidden. (E) Positions and orientations of positively charged residues in the belt based on AlphaFold models of GSDMB-NTs. A hypothetical membrane is shown in gray. The positively charged residues are shown as blue sticks in GSDMB3-NT244 and GSDMB4-NT, as well as green sticks in other isoforms. (F) Membrane lipid strips (top) were incubated with indicated proteins, and binding was assessed by blotting for GSDMB (bottom). (G) HEK293T cells, transfected with indicated plasmids, were lysed and resolved on a native gel (top) and an SDS-PAGE (bottom), immunoblotted for GSDMB. (H and I) HEK293T cells, transiently transfected with the indicated amount of plasmids (2X, two times the plasmid compared with GSDMB3-NT244; 4X, four times), were assessed 24 hours after transfection for pyroptosis by LDH release (H) and GSDMB expression by immunoblots (I). Data are mean ± SD of biological triplicates and are representative of at least two independent experiments. Comparisons were calculated by two-tailed Student's *t* test. **P* < 0.05 and ***P* < 0.01.

of cell death. Unexpectedly, oligomers were detected in all noncytotoxic GSDMB-NTs, including B1, B2, B3S, and B5, suggesting that the belt does not markedly contribute to GSDMB-NT oligomerization. Our results contrast with mutagenesis experiments and molecular dynamics simulations pointing toward the involvement of the belt in GSDMB-NT oligomerization (30, 31, 33).

Because noncytotoxic GSDMB-NTs still bind lipids and oligomerize (Fig. 2, F and G), we reasoned that the pore formation process is arrested at the insertion. Before membrane insertion, GSDM-NTs oligomerize into prepores, arcs, and slits (9, 26, 34, 35). The belt likely contributes to the insertion of the oligomeric GSDMB-NTs. If so, then one would expect that noncytotoxic GSDMB-NTs impair the pore-forming abilities of cytotoxic GSDMB-NTs. When we coexpressed cytotoxic GSDMB3-NT244 with either GSDMB1-NT or GSDMB2-NT in HEK293 cells,

pyroptosis was dampened in a dose-dependent, dominant-negative manner, manifested by notably reduced LDH release (*P* < 0.01) (Fig. 2H). The blockade effect was not due to decreased GSDMB3-NT244 expression, given consistent expression levels shown by immunoblotting (Fig. 2I). Likewise, flow cytometry experiments using mCherry as an indicator of GSDMB3-NT244 expression similarly showed dampened SYTOX uptake at the same levels of GSDMB3-NT244 in the presence of noncytotoxic isoforms (Fig. 2H and fig. S2). Together, our data indicate that the belt facilitates the membrane insertion of membrane-bound, oligomeric GSDMB-NTs. Exact mechanisms of blockade by noncytotoxic GSDMBs await further investigation. Indirect mechanisms may exist such as competition among GSDMBs for activating proteases and membrane lipids.

GSDMB isoforms are heterogeneously expressed

To better understand the functional importance of GSDMB splicing, we profiled the expression of endogenous GSDMB isoforms in a panel of cell lines including cancer lines. One pair of primers (F1/R1) was designed to detect total GSDMB expression, and another pair (F2/R2) flanking exons 6 and 7 was used to detect GSDMB variants (Fig. 3A). Total GSDMB expression was analyzed by quantitative reverse transcription polymerase chain reaction (qRT-PCR) using F1/R1 primers (Fig. 3B). All these cell lines expressed GSDMB to different degrees. Colorectal adenocarcinoma SW837, SW1116, and HT29 showed the highest endogenous GSDMB expression. Hepatocellular carcinoma HepG2, neuroblastoma SH-SY5Y, and lung carcinoma A549 cells showed moderate expression, whereas the other cells had minimal expression. HeLa had the lowest expression, about threefold lower than the low-expressing cell lines. Using flanking primers F2/R2 to probe cDNAs from these cells, we detected five bands at different molecular weights

corresponding to GSDMB isoforms 1 to 5 by size (Fig. 3C). Sanger sequencing of these bands in SW1116 and HepG2 cells confirmed that GSDMB isoforms 1 to 4 were expressed in these cells (fig. S3). However, instead of GSDMB5, an out-of-frame variant (named GSDMB6 hereafter) containing a 13-nucleotide deletion in exon 6 was identified. GSDMB6 is a 237-amino acid truncated fragment, which lacks a stable belt and should therefore be noncytotoxic, similar to GSDMB5 (Fig. 2, A and D). Among the six variants, GSDMB1/2/3 were abundant isoforms, and GSDMB4/6 were much less abundant, whereas GSDMB5 was not detected in our experiments. We therefore focused on the two abundant noncytotoxic isoforms, GSDMB1/2, and two cytotoxic isoforms, GSDMB3/4, hereafter.

Because HeLa cells barely express endogenous GSDMB (Fig. 3B), they are an ideal model for studying GSDMB isoforms in an over-expression setting. We stably overexpressed GSDMB isoforms 1 to 4 in HeLa cells individually, using an empty vector (EV) construct as a

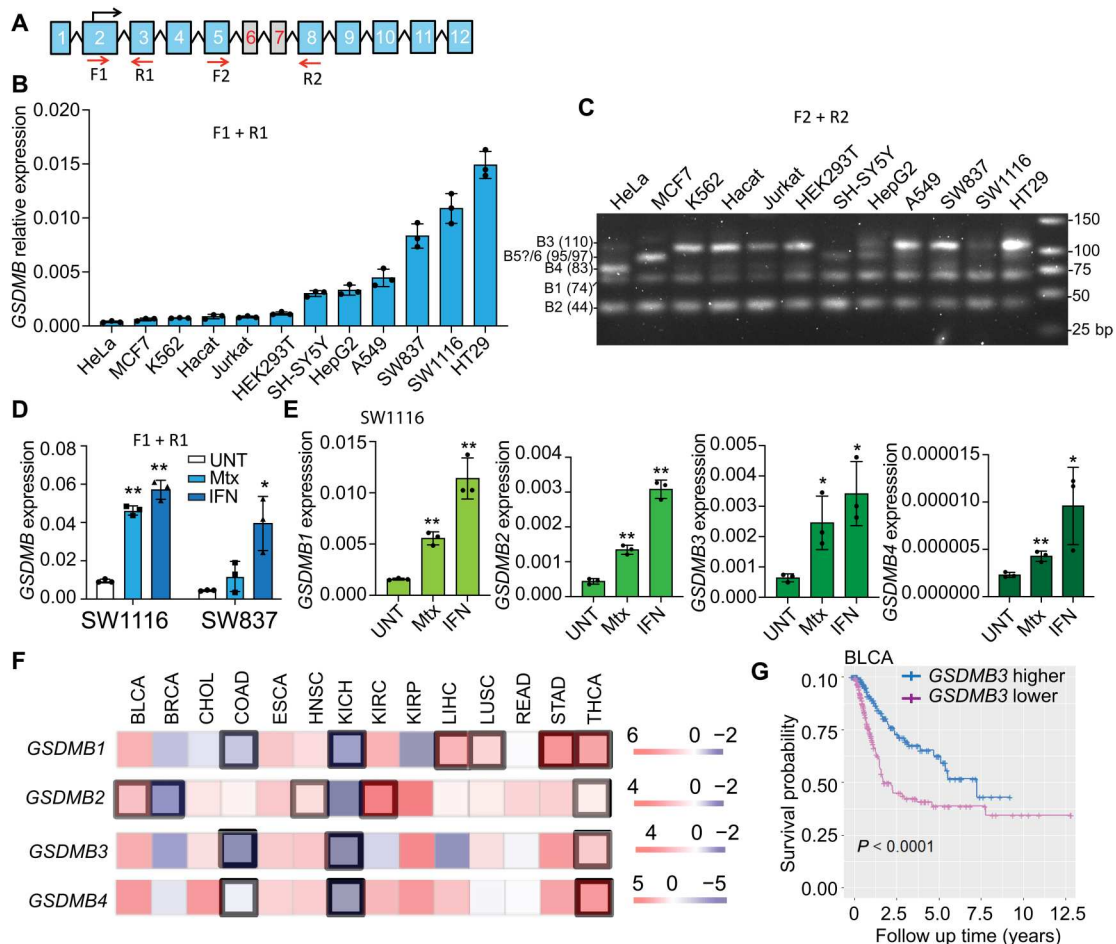


Fig. 3. Expression of GSDMB isoforms. (A) Schematic of the PCR primers used to detect total GSDMB (F1/R1) or specific isoforms (F2/R2). (B) Expression of GSDMB in indicated cell lines, assessed by qRT-PCR using F1/R1 primers, relative to *glyceraldehyde-3-phosphate dehydrogenase*. (C) PCR products of GSDMB isoforms, resolved on 3% agarose gels, were amplified using F2/R2 primers. (D) Effect of IFN- γ and Mtx on total GSDMB expression in SW837 and SW1116 cells, assessed by qRT-PCR with F1/R1 primers. (E) Effect of IFN- γ and Mtx on the expression of GSDMB isoforms in SW1116 cells, assessed by qRT-PCR with isoform-specific primers. (F) Expression of GSDMB isoforms in primary tumors compared with adjacent normal tissue in the Cancer DEIso and TCGA database. Comparisons were calculated by paired Wilcoxon test, and $P < 0.01$ was considered significant (highlighted in black boxes). (G) Correlation of GSDMB3 expression and survival in patients with BLCA. Data in (B) and (D) are mean \pm SD of biological triplicates and are representative of three independent experiments. Statistical analysis was performed using the two-tailed Student's t test. ** $P < 0.01$ and * $P < 0.05$.

control. Anti-GSDMB immunoblotting showed that those isoforms were comparably expressed (fig. S4A). Isoform-specific primers detected the expected GSDMB isoforms in HeLa *GSDMB1-4* cells, but not in the EV control (fig. S4B).

GSDMBs are differentially regulated in cancers and linked to survival outcomes

GSDMB is highly expressed in SW837 and SW1116 colorectal carcinoma cells. Its expression can be transcriptionally up-regulated by IFN- γ in those cells (13). Methotrexate (Mtx) treatment also induces *GSDMB* expression (15). *GSDMB* proteins induced by IFN- γ and Mtx have been reported to concentrate in different cellular compartments and regulate cell proliferation and migration (15). We confirmed that *GSDMB* could be significantly ($P < 0.01$) induced by both IFN- γ and Mtx in SW1116 cells but only by IFN- γ in SW837 cells (Fig. 3D). To test whether these two stimuli up-regulate different *GSDMB* isoforms in SW1116 cells, we performed qRT-PCR using isoform-specific primers on treated SW1116 cells. All four isoforms were induced by both IFN- γ and Mtx in SW1116 cells (Fig. 3E), although less so by Mtx, suggesting that their expression is similarly regulated.

Nonetheless, when comparing *GSDMB* isoform expression in tumors with that in adjacent normal tissues using the Cancer DEIso and the Cancer Genome Atlas (TCGA) databases (Fig. 3F), we found that the expression of *GSDMB* isoforms is differentially regulated in tumors. Our bioinformatics analysis showed that noncytotoxic *GSDMB2* expression is significantly up-regulated in multiple tumor types ($P < 0.01$), including bladder urothelial carcinoma (BLCA), head and neck squamous cell carcinoma (HNSC), kidney renal clear cell carcinoma (KIRC), and thyroid carcinoma (THCA) but considerably reduced in breast invasive carcinoma (BRCA) compared with adjacent normal tissues. Similarly, *GSDMB1* is up-regulated considerably in four tumor types but suppressed in two other tumor types (Fig. 3F). Cytotoxic *GSDMB3/4* are simultaneously down-regulated in colon adenocarcinoma (COAD) and kidney chromophobe tumors (KICH) but up-regulated only in THCA (Fig. 3F). These data indicate that noncytotoxic *GSDMB1/2* may be more likely to be overexpressed, whereas cytotoxic *GSDMB3/4* is suppressed in primary tumors, suggesting opposite roles in tumor development. We also verified the expression of *GSDMB* isoforms in some TCGA primary tumors compared with the Genotype-Tissue Expression (GTEx) normal tissue in the UCSC Xena database (fig. S5). We found that most of our expression data can be reproduced, except that *GSDMB1* and *GSDMB4* are not differentially expressed in KICH and THCA, respectively, and that *GSDMB2* is reduced in THCA compared with normal tissues. However, these results do not contradict the observed expression trends of *GSDMB* isoforms in primary tumors. When analyzing the effect of tumor expression of *GSDMB* on patient survival, significant differences in survival ($P < 0.01$) were observed only in patients with BLCA and KIRC but not in other patients. In BLCA, increased expression of cytotoxic *GSDMB3* was associated with better survival (Fig. 3G), whereas expression of the other isoforms had little effect on patient survival (fig. S6A). In patients with KIRC, higher expression of any of the four *GSDMB* isoforms, among which only *GSDMB2* was significantly up-regulated (Fig. 3F), was associated with worse survival ($P < 0.01$) (fig. S6B).

Some genomic single-nucleotide polymorphism (SNP) variants also differentially regulate *GSDMB* isoform expression.

Homozygotes for the minor allele of *GSDMB rs11078928* showed almost no expression of exon 6-containing cytotoxic *GSDMB3* and *GSDMB4* isoforms but expressed the noncytotoxic *GSDMB1/2* isoforms (36). Another minor variant, *GSDMB rs8067378*, has been associated with increased cervical cancer risk in East Asians (37–40). We analyzed those two minor alleles and found that they are closely linked ($R^2 = 0.9951$, $P < 0.0001$ in East Asians), meaning that most people carry both or neither of these two minor alleles. This observation suggests that loss of cytotoxic *GSDMB* isoforms in *rs11078928* is associated with higher cervical cancer risk. These data together suggest that expression of cytotoxic *GSDMB3/4* may correlate with better clinical outcomes and reduced tumor risk, whereas noncytotoxic *GSDMB1/2* is frequently overexpressed in tumors and may exert functions that promote tumor development.

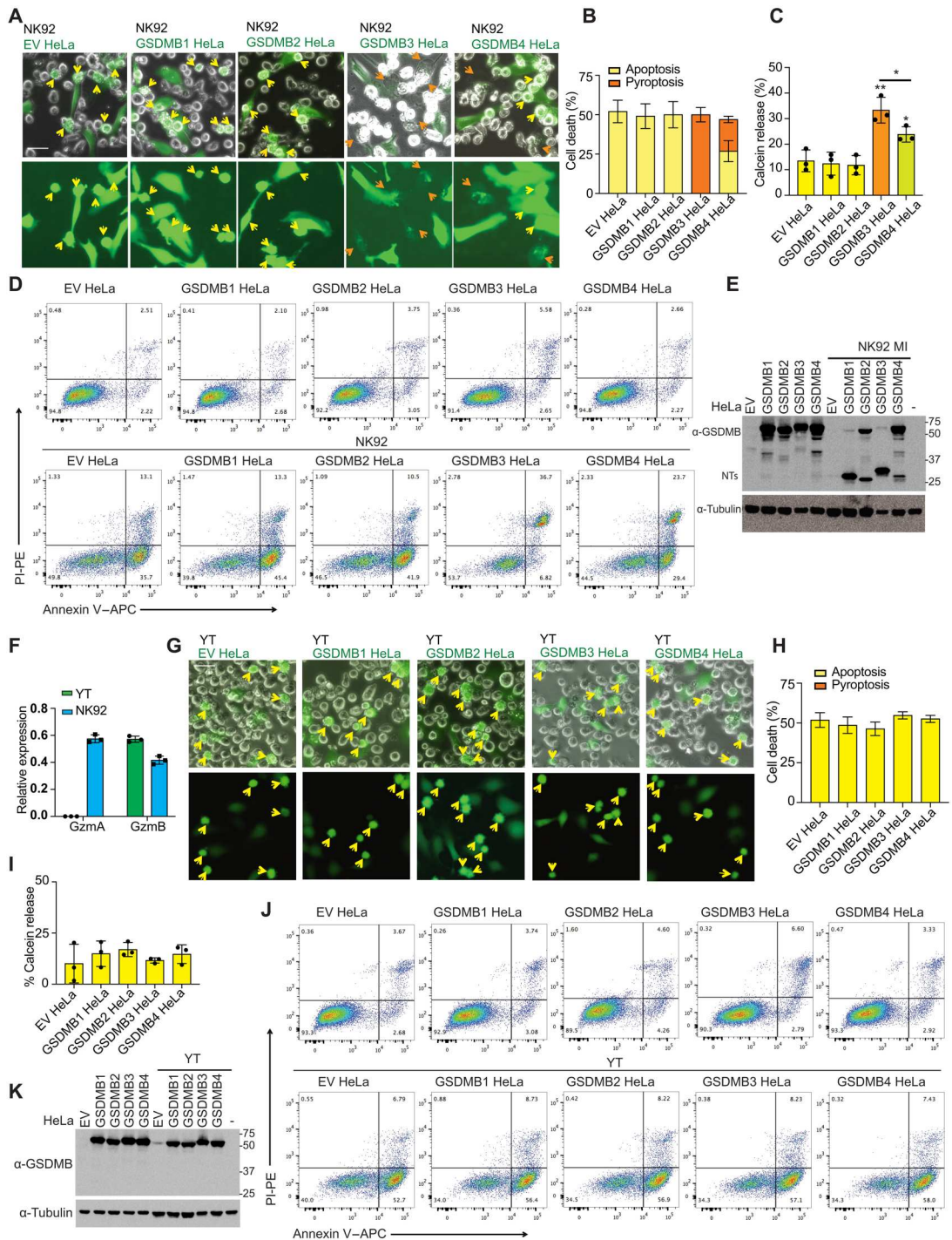
Pyroptosis-independent functions of GSDMB may be context specific

We next investigated previously described pyroptosis-independent functions of GSDMB. *GSDMB1* has been reported to be nuclear localized and to function as a transcription activator (21), although other studies reported cytosolic localization of *GSDMB* (15). To assess cellular localization, we expressed CT green fluorescent protein (GFP)-tagged *GSDMB* isoforms in HeLa cells, and their localization was determined by confocal microscopy (fig. S7A). All the ectopically expressed *GSDMB* isoforms were distributed to both the cytoplasm and the nuclei of HeLa cells, and none were exclusively in the nucleus. We further tested whether *GSDMBs* function as transcription activators in *GSDMB*-expressing HeLa cells by examining the expression of *5-lipoxygenase (5-LO)* and *transforming growth factor- β 1 (TGF- β 1)*, which have been shown to be up-regulated by *GSDMB* in human bronchial epithelial cells (21). Compared with HeLa cells expressing EV, HeLa cells overexpressing *GSDMB* isoforms did not show different *TGF- β 1* expression but showed markedly reduced *5-LO* expression (fig. S7B). We next tested whether *GSDMBs* promote tumor cell proliferation and migration as reported (15, 19, 20). In HeLa cells, proliferation rates, colony formation, and cell migration were unchanged by ectopic *GSDMB1-4* expression compared with cells transfected with an EV control (fig. S7, C to F). These data suggest that the reported nonpyroptotic roles of *GSDMB* in transcriptional activation, cell proliferation, and migration may be limited to certain cells and contexts.

GSDMB isoforms 3 and 4 induce pyroptosis during killer lymphocyte attacks

Killer lymphocytes activate pyroptosis in *GSDMB*-expressing target cells by GzmA release but activate caspase-independent noninflammatory cell death, apoptosis, in targets that do not express *GSDMB* (13). To test whether *GSDMB* isoforms are differentially activated by killer cells, the human NK (hNK) cell line NK-92 MI was incubated with target HeLa cells stably expressing *GSDMB1-4* or EV (fig. S4) and loaded with calcein AM (acetoxymethyl), a cell membrane-permeable dye released only when the cell membrane is disrupted (Fig. 4, A to E) (41). Pyroptosis causes rapid membrane permeabilization with characteristic cell membrane ballooning, whereas apoptosis features cell shrinking, DNA condensation, and cell membrane blebbing, with delayed cell membrane disruption. After 2.5 hours, NK-92 MI cocultures with HeLa cells

Fig. 4. GSDMB3 and GSDMB4 mediate GzmA-triggered pyroptosis. (A and B) Representative fluorescent microscopy images of cocultures of NK-92 MI cells with calcein-labeled (green) EV and GSDMB-expressing HeLa cells (A). Yellow arrows indicate apoptotic cells, and orange arrows indicate pyroptotic cells. The percentage of dead cells was counted and quantified using three images (B). (C) Calcein release of EV and GSDMB-expressing HeLa cells induced by NK-92 MI cells (E/T ratio = 3/1; 2.5 hours). (D) Indicated HeLa cells were co-incubated with NK-92 MI cells at the E/T ratio of 3/1 for 2.5 hours. Cell death was assessed by annexin V/PI staining and flow cytometry. (E) GSDMB cleavage in GSDMB-expressing HeLa cells incubated with NK-92 MI cells at the E/T ratio of 3/1 for 2.5 hours, assessed by immunoblotting. (F) Expression of GzmA and GzmB in YT-INDY and NK-92 MI cells, assessed by qRT-PCR. (G and H) Representative fluorescent microscopy images of cocultures of YT NK cells with calcein-labeled (green) EV and GSDMB-expressing HeLa cells (G). Yellow arrows indicate apoptotic cells. The percentage of dead cells was counted and quantified from three images (H). (I) Calcein release of EV and GSDMB-expressing HeLa cells induced by YT cells (E/T ratio = 3/1; 2.5 hours). (J) Indicated HeLa cells were co-incubated with YT cells at the E/T ratio of 3/1 for 2.5 hours. Cell death was assessed by annexin V/PI staining and flow cytometry. (K) GSDMB cleavage in GSDMB HeLa cells incubated with YT cells at the E/T ratio of 3/1 for 2.5 hours, assessed by immunoblotting. Data in bar graphs are mean ± SD of biological triplicates and are representative of three independent experiments. Comparisons were calculated by two-tailed Student's *t* test. ***P* < 0.01 and **P* < 0.05. Scale bar, 20 μm.



expressing EV, GSDMB1, and GSDMB2 contained dying HeLa cells with apoptotic features and bright calcein staining, indicating that isoforms 1 and 2 did not trigger pyroptosis (Fig. 4, A and B). In contrast, there were many pyroptotic HeLa cells expressing GSDMB3, which had cell membrane balloons and released calcein. Both apoptotic and pyroptotic cells were observed in GSDMB4-expressing HeLa cells. Quantification confirmed that

only GSDMB3- and GSDMB4-expressing HeLa cells released calcein into the supernatant above background (Fig. 4C). To confirm these results, Vybrant DiD, a cell membrane dye, was used to label NK-92 MI-targeted GSDMB-expressing HeLa cells. Giant membrane balloons were again observed in dying GSDMB3-expressing HeLa cells and, to a lesser extent, in GSDMB4-expressing HeLa cells, but not in cells expressing the

other isoforms, which showed shrunken cells dying an apoptotic cell death (fig. S8).

Annexin V/propidium iodide (PI) staining has been widely used to characterize apoptotic cell death. Early apoptotic cells can be stained by annexin V conjugates but not by PI (annexin V⁺/PI⁻) and will eventually become annexin V⁺/PI⁺ and annexin V⁻/PI⁺ when the cell membrane is disrupted by secondary necrosis. By contrast, pyroptotic cells are annexin V⁺/PI⁺ from the beginning of cell death (13). We characterized NK-92 MI–targeted GSDMB-expressing HeLa cells by annexin V/PI staining and flow cytometry analysis by 2.5 hours after coculture, when secondary necrosis rarely occurs (Fig. 4D). Our data indicate that, in EV control HeLa or HeLa cells expressing noncytotoxic GSDMB1 and GSDMB2, most of the dead cells stained annexin V⁺/PI⁻, an indicator of early apoptosis. Whereas in GSDMB3-expressing HeLa cells, most of the dead cells were annexin V⁺/PI⁺, supporting that these cells mainly underwent pyroptosis. GSDMB4-expressing cells contained both annexin V⁺/PI⁻ and annexin V⁺/PI⁺ populations, agreeing with our observation that GSDMB4 cells underwent both apoptosis and pyroptosis. A small annexin V⁺/PI⁺ cell population was observed in control or GSDMB1/2 HeLa cells, presumably because of the secondary necrosis or membrane damage of cells during sample handling.

Next, we assessed GSDMB isoform cleavage in NK-92 MI–treated HeLa cells by immunoblotting (Fig. 4E). A GSDMB-NT band of the expected size was generated after NK attack of the HeLa cells expressing each of the GSDMB isoforms, but uncleaved, FL GSDMB2 and GSDMB4 were prominent in cells expressing those isoforms, suggesting that isoforms 2 and 4 were partially resistant to GzmA cleavage. Therefore, although both GSDMB3-NT244 and GSDMB4-NT are cytotoxic, GSDMB4 is less likely to trigger pyroptosis because of resistance to cleavage by GzmA. To further confirm the NK cell killing results, we treated GSDMB-expressing HeLa cells with primary hNK cells isolated from peripheral blood mononuclear cells (PBMCs; fig. S9A) and assessed cell death by annexin V/PI staining and flow cytometry (fig. S9B). hNK cells rapidly killed ~85% of the target cells in 2.5 hours. Similar to NK-92 MI cells, hNK cells triggered similar types of cell death in HeLa cells expressing four GSDMBs. Thus, GSDMB3 and, to a lesser extent, GSDMB4, but not GSDMB1 or GSDMB2, trigger killer lymphocyte-mediated pyroptosis.

Killer cell–triggered GSDMB-induced pyroptosis depends on GzmA

Previous work suggested that GzmA is responsible for GSDMB cleavage and target cell pyroptosis after killer cell attacks (13). To confirm this finding, GSDMB1–4–expressing HeLa cells were challenged with YT-INDY cells, a hNK cell line expressing GzmB but not GzmA (Fig. 4F) (42). Two and a half hours after YT challenge, apoptosis was induced in all GSDMB1–4–expressing and EV control HeLa cells, as indicated by cell shrinkage, membrane blebbing, bright calcein staining, and the absence of membrane balloons (Fig. 4, G and H). Moreover, GSDMB expression did not increase calcein in culture supernatants above background (Fig. 4I) and did not increase annexin V⁺/PI⁺ dead cells in flow cytometry analyses (Fig. 4J). *GZMA*^{-/-} YT attack did not lead to GSDMB cleavage, as assessed by immunoblotting (Fig. 4K). Thus, GzmA is responsible for cleaving GSDMB and triggering pyroptosis in target cells subjected to killer lymphocyte attack.

DISCUSSION

Here, we showed that *GSDMB* splicing variants differ in pore-forming activity and susceptibility to GzmA cleavage. Only GzmA-activated GSDMB3 and GSDMB4 isoforms form cell membrane pores. Therefore, splicing isoforms of *GSDMB* play distinct roles in killer cell–triggered pyroptosis. These data explain the conflicting reports about GSDMB activity. In our study, GSDMB2 and GSDMB4, both of which lack the exon 7–encoded region, were partially resistant to killer cell GzmA-mediated cleavage, in contrast with uniform cleavage of purified recombinant GSDMBs *in vitro* (13). GzmA primarily cleaves after a conserved lysine residue in all GSDMB isoforms (fig. S1), but the sequences preceding this residue vary among isoforms. The different results observed *in vitro* and in cells may reflect distinct protein conformations, post-translational modifications, and concentrations in cells. It is also possible that GSDMB isoforms complex differently with other cellular proteins, which alters their cleavage efficiency in cells.

Whereas we studied six *GSDMB* isoforms, other isoforms have been reported, which encode short truncations or generate a circular RNA (43, 44). Out-of-frame isoforms are generally susceptible to nonsense-mediated RNA decay, a mechanism that prevents the production of truncated proteins in cells (44), and, therefore, their RNAs are unstable in cells. The out-of-frame variant *GSDMB6* we identified encodes a 237–amino acid truncated protein and has very low expression in cells. *GSDMB5* (411 amino acids) has been widely used in GSDMB studies. However, *GSDMB5* is not a major *GSDMB* isoform in the cells tested in our study.

GSDMB is the only GSDM that lacks a mouse counterpart, which hampers the utilization of mouse tumor models to dissect GSDMB function *in vivo*. A recent study used a knock-in strategy to express *GSDMB2* in mice ubiquitously (45). Although expression of *GSDMB2* did not affect the overall frequency of spontaneous neoplasia, coexpression of *GSDMB2* and human epidermal growth factor receptor 2 (HER2) increased the incidence of breast cancer in mice, suggesting that protumor functions of *GSDMB2* could be context dependent. When overexpressing *GSDMB* isoforms in HeLa cells, we did not observe any change in cell proliferation and migration, which could be attributed to a cell type–dependent effect.

Our study suggested that noncytotoxic GSDMB isoforms (such as GSDMB1/2) function as negative regulators of GSDMB-mediated pyroptosis. The NT fragments of noncytotoxic and cytotoxic isoforms bound lipids and oligomerized similarly, but coexpression of noncytotoxic isoforms (GSDMB1/2) dampened GSDMB3-NT244–mediated pyroptosis. Noncytotoxic isoforms (1/2) might oligomerize with the cytotoxic isoforms (3/4), forming heterooligomers to block the concerted conformational transition from intermediate assemblies to membrane pores. Therefore, noncytotoxic isoforms could be used by tumors to down-regulate the pore-forming abilities of cytotoxic isoforms.

Aberrant alternative splicing has been implicated in many aspects of cancer, including angiogenesis, cell proliferation, invasion, metastasis, and generation of neoantigens (46). In primary tumors, cytotoxic *GSDMB3/4* are prone to be down-regulated, but noncytotoxic *GSDMB1/2* are frequently up-regulated, suggesting that tumors may use alternative splicing to differentially regulate *GSDMB* isoforms to avoid GSDMB pyroptosis. The splicing alterations of *GSDMB* in tumors could be caused by the occurrence of

cancer driver mutations in genes encoding components of the splicing machinery or genetic mutations at the splicing sites. The minor allele of *GSDMB* rs11078928 alters a splicing site and leads to down-regulation of cytotoxic *GSDMB* isoforms. The rs11078928 allele is associated with a higher risk of cervical cancer, suggesting that cervical cancer cells may use the *GSDMB* splicing to promote tumorigenesis. In addition, the minor allele of rs11078928 is associated with a lower risk of asthma (14), suggesting that *GSDMB*-mediated pyroptosis might also contribute to the pathogenesis of asthma.

Expression of the fully functional *GSDMB3* is associated with better patient survival rates in cancer patients with BLCA. However, the survival of patients with KIRC negatively correlated with the expression of any *GSDMB* isoform. Our and other studies suggest that whether *GSDMB3* expression correlates with better survival in patients is not only determined by *GSDMB3* alone but also by other *GSDMB* isoforms. Although *GSDMB3* mediates killer lymphocyte-triggered pyroptosis that enhances antitumor immunity (13), other studies also suggested that noncytotoxic *GSDMBs*, particularly *GSDMB2*, promoted tumorigenesis by promoting tumor cell proliferation and migration (19, 20). Furthermore, our study revealed that noncytotoxic *GSDMBs* could block antitumor *GSDMB* pyroptosis by interfering with cytotoxic *GSDMBs*. Therefore, the clinical outcomes could be determined by the tug-of-war between the pro- and antitumor functions of different *GSDMB* isoforms. In this case, the fact that *GSDMB3* expression correlates with better survival in BLCA but not KIRC could be due to the different expression levels of other *GSDMB* isoforms in these two tumors. Broadly speaking, because of the heterogeneity of cancers on many levels, including their diverse mechanisms of tumorigenesis and evasion of antitumor immunity, the expression of *GSDMB3* may be antitumor in a cancer type-dependent manner.

From a therapeutic perspective, our data suggest that tumors may manipulate *GSDMB* splicing to avoid pyroptosis. Modulating *GSDMB* splicing to increase cytotoxic *GSDMB* isoforms and suppress noncytotoxic isoforms could improve antitumor immunity and enhance immunotherapy.

MATERIALS AND METHODS

Study design

The objective of this study was to determine whether *GSDMB* splicing variants play distinct roles in killer lymphocyte-mediated pyroptosis and antitumor immunity. To achieve this goal, we have used molecular biological, biochemical, and cellular experiments to show that *GSDMB* isoforms exhibit distinct pore-forming activity and differentially mediate NK cell-triggered pyroptosis. We dissected the underlying molecular mechanism by a combination of structural modeling and biochemical and cellular experiments. Bioinformatics analysis further showed that *GSDMBs* are differentially regulated in cancers and linked to survival outcomes. All experiments were independently repeated at least two or three times, as indicated in figure legends. This study was not blinded.

Cell lines

SW837 (RRID:CVCL_1729) and SW1116 (RRID:CVCL_0544) are from the N. S. laboratory, and all other cells used in this study are from the J. L. laboratory. HeLa (RRID:CVCL_0030), HEK293T (RRID:CVCL_0063), SW837, HaCaT (RRID:CVCL_0038), and MCF7 (RRID:CVCL_0031) were cultured in complete Dulbecco's

modified Eagle's medium as previously reported (10). SW1116, NK-92 MI (RRID:CVCL_3755), YT-Indy (RRID:CVCL_1797), K562 (RRID:CVCL_0004), Jurkat (RRID:CVCL_0065), SH-SY5Y (RRID:CVCL_0019), HepG2 (RRID:CVCL_0027), A549 (RRID:CVCL_0023), and HT29 (RRID:CVCL_0320) cells were cultured in complete RPMI as reported (10). Primary hNK cells were cultured in MACS NK medium with 1% MACS NK supplement (Miltenyi Biotec), 5% serum AB (Sigma-Aldrich), and interleukin-2 (500 IU/ml; Miltenyi Biotec) for 1 to 2 weeks before being used for NK killing assays. All cell lines were verified to be free of mycoplasma by PCR.

Plasmids

pLVX-puro-*GSDMB1-5* plasmids were synthesized by GenScript. *GSDMB1-5* NTs were amplified by PCR from the mentioned plasmids and cloned into c-FLAG pcDNA3 (Addgene) using XhoI and BamHI. A GFP fragment was amplified from the pWPI vector (Addgene) and inserted into pLVX-puro *GSDMB1-4* plasmids using XhoI and NEBuilder HiFi DNA Assembly Master Mix. To express *GSDMB-NT* proteins in *E. coli*, *GSDMB1-5* NTs were cloned into the pET28a vector using XhoI and BamHI. A mutation was introduced into those pET28a-*GSDMB-NT* plasmids to inactivate the NT His tags by quick change PCR using primers 5'-actgttg-gacagcaataaggtcgcggatccatgttc-3' and 5'-gacatggatccgcgacctattgctgtccaccagt-3'. All plasmids were verified by Sanger sequencing.

Generation of stable cell lines

For lentivirus generation, pLVX-Puro-*GSDMB* plasmids were transfected into HEK293T cells with pSPAX2 and pCMV-VSV-G at a 2:2:1 ratio. Supernatants collected 2 days later were used to transduce HeLa for 48 hours. Puromycin (2 µg/ml; Sigma-Aldrich) was then added to select *GSDMB*-positive cells. pLVX-Puro EV was used to generate the control cells.

Semiquantitative and quantitative RT-PCR

For *GSDMB* induction, cells were treated with IFN-γ (10 ng/ml) or 10 µM Mtx for 48 hours. RNA was extracted using TRIzol reagent (Life Technologies) according to the manufacturer's instructions and was subject to reverse transcription using M-MLV reverse transcriptase (Invitrogen). *GSDMB*, *TGF-β1* and *5-LO* expression were determined by qRT-PCR using iTaq Universal SYBER Green Supermix (Bio-Rad).

Sanger sequencing for *GSDMB* isoforms

A F2/R2 primer pair was used to amplify the different *GSDMB* isoforms from SW1116 and HepG2 cDNA. Then, gel purification was performed using the QIAquick gel purification kit (QIAGEN, 28706) for the PCR products (40 to 120 base pairs) on agarose gel. Purified PCR products were cloned into the pCR2.1-TOPO vector (Invitrogen, 45-0245), and plasmid DNAs were extracted for Sanger sequencing.

Cytotoxicity assay in HEK293T cells

The transfection and LDH release in HEK293T were performed as reported (10). Pyroptotic cells were imaged using the EVOS FL cell imaging system. Alternatively, cells were stained with SYTOX Green (Invitrogen, R37168) and analyzed on a CytoFLEX flow cytometer (Beckman Coulter).

SDS–polyacrylamide gel electrophoresis and native gel immunoblot

SDS–polyacrylamide gel electrophoresis (SDS-PAGE) and native gel immunoblot were performed as previously reported (4). Antibodies used were anti-GSDMB (ab215729, Abcam; RRID:AB_2909483), anti-FLAG (F1804, Sigma-Aldrich; RRID:AB_262044), and anti-tubulin (T5168, Sigma-Aldrich; RRID:AB_477579).

Immunoprecipitation and lipid binding assay

For the purification of CT FLAG-tagged GSDMB-NT proteins by immunoprecipitation, HEK293T cells transiently expressing GSDMB-NT were lysed in lysis buffer (4) containing complete protease inhibitor cocktail (Roche). Lysates were incubated with anti-FLAG M2 beads (Sigma-Aldrich) for 3 hours at 4°C. Beads were washed three times with lysis buffer, and proteins were eluted with lysis buffer containing 3× FLAG peptides (100 µg/ml; Sigma-Aldrich). For lipid binding assays, precipitates were spotted on Membrane Lipid Strips (Echelon Biosciences) according to the manufacturer's instructions.

Isolation of primary NK cells

hNK cells were isolated from human PBMCs using the hNK Cell Isolation Kit (Miltenyi Biotec) according to the manufacturer's instructions. Isolated NK cells were accessed using anti-CD56 (BioLegend, catalog no. 362507) and anti-CD3 (BioLegend, catalog no. 300306) staining and flow cytometry.

NK cell killing assay

For NK cell-induced cell death, HeLa cells were seeded in 24-well plates overnight. Cells were loaded with 5 µM calcein AM (eBioscience) before co-incubating with NK-92 MI, YT, or primary NK cells at E:T ratios = 3:1. Two and a half hours after incubation, calcein release was determined by recording fluorescence at 528 nM after excitation at 485 nM using a BioTek Synergy plate reader. For flow cytometry analysis, cells were collected by trypsinization and stained with annexin V conjugates (Thermo Fisher Scientific, A23204) and PI (Abcam). Samples were immediately analyzed by flow cytometry. For Vybrant DiD staining, HeLa cells were seeded overnight and stained with Vybrant DiD dye (Thermo Fisher Scientific) according to the manufacturer's instructions, and then NK-92 MI cells were added at an E:T ratio of 3:1. Pyroptotic cells were imaged using the EVOS FL cell imaging system.

Bacterial killing assay

For the cytotoxicity of N termini of GSDMB isoforms in *E. coli*, 50 µl of BL21 cells (DE3, Thermo Fisher Scientific, EC0114) were transformed with a pET28a-GSDMB-NT plasmid (100 ng) and plated equally on kanamycin-containing LB plates with or without 0.1 M IPTG. The plates were incubated overnight at 37°C before the colony-forming units were determined.

GSDMB localization

HeLa cells stably expressing GSDMB-GFP were seeded in 12-well plates. The next day, cells were washed with phosphate-buffered saline (PBS) twice and fixed with cold 100% methanol for 10 min at –20°C. The cells were washed twice with PBS and stained with 4',6-diamidino-2-phenylindole (1 µg/ml; Abcam) for 10 min at room temperature, then washed with PBS and mounted with

VECTASHIELD antifade mounting medium (Vector Laboratories, catalog no. H-1200-10). Z-stack images (63×) were acquired with a Zeiss LSM 880 confocal microscope and processed with Fiji software.

Proliferation, colony formation, and wound healing assays

Proliferation was measured using the CellTiter-Glo ATP viability kit (Promega) according to the manufacturer's instructions. Colony formation assay was performed using crystal violet staining. Wound healing assay (Abcam) was performed according to the manufacturer's instructions. Images were taken by the EVOS FL cell imaging system and analyzed by ImageJ.

Bioinformatics analysis

Isoform-level expression information based on fragments per kilobase of transcript per million mapped reads (FPKM) regarding four GSDMB isoforms (NM_001042471, NM_001165958, NM_001165959, and NM_018530) was obtained from Cancer DEIso (47). We got 19 tumor samples and 19 matched normal samples in TCGA-BLCA (T19 N19), 111 paired samples in TCGA-BRCA, 9 paired samples in TCGA-CHOL, 40 paired samples in TCGA-COAD, 6 paired samples in TCGA-ESCA, 42 paired samples in TCGA-HNSC, 23 paired samples in TCGA-KICH, 72 paired samples in TCGA-KIRC, 31 paired samples in TCGA-KIRP, 42 paired samples in TCGA-LIHC, 49 paired samples in TCGA-LUSC, 9 paired samples in TCGA-READ, 26 paired samples in TCGA-STAD, and 58 paired samples in TCGA-THCA. To identify differentially expressed isoforms between tumors and adjacent normal tissues in these cancers, we performed a paired Wilcoxon test for each isoform of GSDMB. *P* values of < 0.01 were considered significant.

To verify the expression of GSDMB isoforms in BLCA, KICH, and THCA, we used TCGA and GTEx samples in the UCSC Xena. Besides samples in TCGA, normal tissue samples whose sources are "Bladder," "Kidney," and "Thyroid" in GTEx were used as additional TCGA-BLCA, TCGA-KICH, and TCGA-THCA normal samples, respectively. We got 406 tumor and 27 normal samples in TCGA-BLCA, 65 tumor and 24 normal samples in TCGA-KICH, and 510 tumor and 337 normal samples in TVGA-THCA. Processed RNA-seq by expectation maximization (RSEM) expected count of transcript expression across samples was recomputed using the UCSC TOIL RNA-seq pipeline and extracted from the Xena browser. Unpaired Wilcoxon tests were performed on TCGA tumors (TCGA sample size is more), TCGA normal, and GTEx normal tissues.

For survival analysis, we collected tumor samples from 406 patients with BLCA and tumor samples from 527 patients with KIRC and defined those samples in which isoform expression was greater than median expression across samples as the higher group; otherwise, they were sorted into the lower group. We did the survival analysis between the higher and lower group across cancers on the basis of log rank test. *P* values of <0.01 were considered significant.

Statistics

Student's *t* test (two-tailed), paired-samples Wilcoxon signed-rank test, unpaired Wilcoxon rank sum test, or log-rank test was used to determine differences between two groups as indicated in the figure

captions. *P* values of <0.05 were considered significant (unless stated otherwise) and are shown in figures.

Supplementary Materials

This PDF file includes:

Figs. S1 to S9
Table S1

Other Supplementary Material for this manuscript includes the following:

Data file S1
MDAR Reproducibility Checklist

[View/request a protocol for this paper from Bio-protocol.](#)

REFERENCES AND NOTES

- X. Liu, S. Xia, Z. Zhang, H. Wu, J. Lieberman, Channelling inflammation: Gasdermins in physiology and disease. *Nat. Rev. Drug Discov.* **20**, 384–405 (2021).
- X. Shi, Y. Zhao, K. Wang, X. Shi, Y. Wang, H. Huang, Y. Zhuang, T. Cai, F. Wang, F. Shao, Cleavage of GSDMD by inflammatory caspases determines pyroptotic cell death. *Nature* **526**, 660–665 (2015).
- N. Kayagaki, I. B. Stowe, B. L. Lee, K. O'Rourke, K. Anderson, S. Warming, T. Cuellar, B. Haley, M. Roose-Girma, Q. T. Phung, P. S. Liu, J. R. Lill, H. Li, J. Wu, S. Kummerfeld, J. Zhang, W. P. Lee, S. J. Snipas, G. S. Salvesen, L. X. Morris, L. Fitzgerald, Y. Zhang, E. M. Bertram, C. C. Goodnow, V. M. Dixit, Caspase-11 cleaves gasdermin D for non-canonical inflammasome signalling. *Nature* **526**, 666–671 (2015).
- X. Liu, Z. Zhang, J. Ruan, Y. Pan, V. G. Magupalli, H. Wu, J. Lieberman, Inflammasome-activated gasdermin D causes pyroptosis by forming membrane pores. *Nature* **535**, 153–158 (2016).
- J. Ding, K. Wang, W. Liu, Y. She, Q. Sun, J. Shi, H. Sun, D.-C. Wang, F. Shao, Pore-forming activity and structural autoinhibition of the gasdermin family. *Nature* **535**, 111–116 (2016).
- L. Sborgi, S. Rühl, E. Mulvihill, J. Pipercevic, R. Heilig, H. Stahlberg, C. J. Farady, D. J. Müller, P. Broz, S. Hiller, GSDMD membrane pore formation constitutes the mechanism of pyroptotic cell death. *EMBO J.* **35**, 1766–1778 (2016).
- X. Chen, W.-T. He, L. Hu, J. Li, Y. Fang, X. Wang, X. Xu, Z. Wang, K. Huang, J. Han, Pyroptosis is driven by non-selective gasdermin-D pore and its morphology is different from MLKL channel-mediated necroptosis. *Cell Res.* **26**, 1007–1020 (2016).
- R. A. Aglietti, A. Estevez, A. Gupta, M. G. Ramirez, P. S. Liu, N. Kayagaki, C. Ciferri, V. M. Dixit, E. C. Dueber, GsdmD p30 elicited by caspase-11 during pyroptosis forms pores in membranes. *Proc. Natl. Acad. Sci. U.S.A.* **113**, 7858–7863 (2016).
- S. Xia, Z. Zhang, V. G. Magupalli, J. L. Pablo, Y. Dong, S. M. Vora, L. Wang, T.-M. Fu, M. P. Jacobson, A. Greka, J. Lieberman, J. Ruan, H. Wu, Gasdermin D pore structure reveals preferential release of mature interleukin-1. *Nature* **593**, 607–611 (2021).
- Z. Zhang, Y. Zhang, S. Xia, Q. Kong, S. Li, X. Liu, C. Junqueira, K. F. Meza-Sosa, T. M. Y. Mok, J. Ansara, S. Sengupta, Y. Yao, H. Wu, J. Lieberman, Gasdermin E suppresses tumour growth by activating anti-tumour immunity. *Nature* **579**, 415–420 (2020).
- Z. Zhang, Y. Zhang, J. Lieberman, Lighting a fire: Can we harness pyroptosis to ignite antitumor immunity? *Cancer Immunol. Res.* **9**, 2–7 (2021).
- Q. Kong, Z. Zhang, Cancer-associated pyroptosis: A new license to kill tumor. *Front. Immunol.* **14**, 1082165 (2023).
- Z. Zhou, H. He, K. Wang, X. Shi, Y. Wang, Y. Su, Y. Wang, D. Li, W. Liu, Y. Zhang, L. Shen, W. Han, L. Shen, J. Ding, F. Shao, Granzyme A from cytotoxic lymphocytes cleaves GSDMD to trigger pyroptosis in target cells. *Science* **368**, eaaz7548 (2020).
- R. A. Panganiban, M. Sun, A. Dahlin, H.-R. Park, M. Kan, B. E. Himes, J. A. Mitchell, C. Iribarren, E. Jorgenson, S. H. Randell, E. Israel, K. Tantisira, S. Shore, J.-A. Park, S. T. Weiss, A. C. Wu, Q. Lu, A functional splice variant associated with decreased asthma risk abolishes the ability of gasdermin B to induce epithelial cell pyroptosis. *J. Allergy Clin. Immunol.* **142**, 1469–1478.e2 (2018).
- N. Rana, G. Privitera, H. C. Kondolf, K. Bulek, S. Lechuga, C. de Salvo, D. Corridoni, A. Antanaviciute, R. L. Maywald, A. M. Hurtado, J. Zhao, E. H. Huang, X. Li, E. R. Chan, A. Simmons, G. Bamias, D. W. Abbott, J. D. Heaney, A. I. Ivanov, T. T. Pizarro, GSDMB is increased in IBD and regulates epithelial restitution/repair independent of pyroptosis. *Cell* **185**, 283–298.e17 (2022).
- Q. Chen, P. Shi, Y. Wang, D. Zou, X. Wu, D. Wang, Q. Hu, Y. Zou, Z. Huang, J. Ren, Z. Lin, X. Gao, GSDMB promotes non-canonical pyroptosis by enhancing caspase-4 activity. *J. Mol. Cell Biol.* **11**, 496–508 (2019).
- J. M. Hansen, M. F. de Jong, Q. Wu, L.-S. Zhang, D. B. Heisler, L. T. Alto, N. M. Alto, Pathogenic ubiquitination of GSDMB inhibits NK cell bactericidal functions. *Cell* **184**, 3178–3191.e18 (2021).
- H. Komiyama, A. Aoki, S. Tanaka, H. Maekawa, Y. Kato, R. Wada, T. Maekawa, M. Tamura, T. Shiroishi, Alu-derived cis-element regulates tumorigenesis-dependent gastric expression of GASDERMIN B (GSDMB). *Genes Genet.* **85**, 75–83 (2010).
- M. Hergueta-Redondo, D. Sarrió, Á. Molina-Crespo, R. Vicario, C. Bernadó-Morales, L. Martínez, A. Rojo-Sebastián, J. Serra-Musach, A. Mota, Á. Martínez-Ramírez, M. Á. Castilla, A. González-Martin, S. Pernas, A. Cano, J. Cortes, P. G. Nuciforo, V. Peg, J. Palacios, M. Á. Pujana, J. Arribas, G. Moreno-Bueno, Gasdermin B expression predicts poor clinical outcome in HER2-positive breast cancer. *Oncotarget* **7**, 56295–56308 (2016).
- M. Hergueta-Redondo, D. Sarrió, Á. Molina-Crespo, D. Megias, A. Mota, A. Rojo-Sebastian, P. García-Sanz, S. Morales, S. Abril, A. Cano, H. Peinado, G. Moreno-Bueno, Gasdermin-B promotes invasion and metastasis in breast cancer cells. *PLOS ONE* **9**, e90099 (2014).
- S. Das, M. Miller, A. K. Beppu, J. Mueller, M. D. McGeough, C. Vuong, M. R. Karta, P. Rosenthal, F. Chouiali, T. A. Doherty, R. C. Kurten, Q. Hamid, H. M. Hoffman, D. H. Broide, GSDMB induces an asthma phenotype characterized by increased airway responsiveness and remodeling without lung inflammation. *Proc. Natl. Acad. Sci. U.S.A.* **113**, 13132–13137 (2016).
- Y. Wang, W. Gao, X. Shi, J. Ding, W. Liu, H. He, K. Wang, F. Shao, Chemotherapy drugs induce pyroptosis through caspase-3 cleavage of a gasdermin. *Nature* **547**, 99–103 (2017).
- C. Rogers, T. Fernandes-Alnemri, L. Mayes, D. Alnemri, G. Cingolani, E. S. Alnemri, Cleavage of DFNA5 by caspase-3 during apoptosis mediates progression to secondary necrotic/pyroptotic cell death. *Nat. Commun.* **8**, 14128 (2017).
- K. L. Chao, L. Kulakova, O. Herzberg, Gene polymorphism linked to increased asthma and IBD risk alters gasdermin-B structure, a sulfatide and phosphoinositide binding protein. *Proc. Natl. Acad. Sci. U.S.A.* **114**, E1128–E1137 (2017).
- M. Mirdita, K. Schütze, Y. Moriwaki, L. Heo, S. Ovchinnikov, M. Steinegger, ColabFold: Making protein folding accessible to all. *Nat. Methods* **19**, 679–682 (2022).
- J. Ruan, S. Xia, X. Liu, J. Lieberman, H. Wu, Cryo-EM structure of the gasdermin A3 membrane pore. *Nature* **557**, 62–67 (2018).
- Z. Liu, C. Wang, J. Yang, B. Zhou, R. Yang, R. Ramachandran, D. W. Abbott, T. S. Xiao, Crystal structures of the full-length murine and human gasdermin D reveal mechanisms of autoinhibition, lipid binding, and oligomerization. *Immunity* **51**, 43–49.e4 (2019).
- Z. Liu, C. Wang, J. Yang, Y. Chen, B. Zhou, D. W. Abbott, T. S. Xiao, Caspase-1 engages full-length gasdermin D through two distinct interfaces that mediate caspase recruitment and substrate cleavage. *Immunity* **53**, 106–114.e5 (2020).
- X. Lei, Z. Zhang, X. Xiao, J. Qi, B. He, J. Wang, Enterovirus 71 inhibits pyroptosis through cleavage of gasdermin D. *J. Virol.* **91**, e01069-17 (2017).
- C. Wang, S. Shivcharan, T. Tian, S. Wright, D. Ma, J. Y. Chang, K. Li, K. Song, C. Xu, V. A. Rathinam, J. Ruan, Structural basis for GSDMB pore formation and its targeting by IpaH7.8. *Nature* 10.1038/s41586-023-05832-z, (2023).
- X. Zhong, H. Zeng, Z. Zhou, Y. Su, H. Cheng, Y. Hou, Y. She, N. Feng, J. Wang, F. Shao, J. Ding, Structural mechanisms for regulation of GSDMB pore-forming activity. *Nature* 10.1038/s41586-023-05872-5, (2023).
- H. Yin, J. Zheng, Q. He, X. Zhang, X. Li, Y. Ma, X. Liang, J. Gao, B. L. Kocsis, Z. Li, X. Liu, N. M. Alto, L. Li, H. Zhang, Insights into the GSDMB-mediated cellular lysis and its targeting by IpaH7.8. *Nat. Commun.* **14**, 61 (2023).
- S. S. Oltra, S. Colomo, L. Sin, M. Pérez-López, S. Lázaro, A. Molina-Crespo, K.-H. Choi, D. Ros-Pardo, L. Martínez, S. Morales, C. González-Paramos, A. Orantes, M. Soriano, A. Hernández, A. Lluch, F. Rojo, J. Albanell, P. Gómez-Puertas, J.-K. Ko, D. Sarrió, G. Moreno-Bueno, Distinct GSDMB protein isoforms and protease cleavage processes differentially control pyroptotic cell death and mitochondrial damage in cancer cells. *Cell Death Differ.* 10.1038/s41418-023-01143-y, (2023).
- E. Mulvihill, L. Sborgi, S. A. Mari, M. Pfreundschuh, S. Hiller, D. J. Müller, Mechanism of membrane pore formation by human gasdermin-D. *EMBO J.* **37**, e98321 (2018).
- S. A. Mari, K. Pluhackova, J. Pipercevic, M. Leipner, S. Hiller, A. Engel, D. J. Müller, Gasdermin-A3 pore formation propagates along variable pathways. *Nat. Commun.* **13**, 2609 (2022).
- F. S. Morrison, J. M. Locke, A. R. Wood, M. Tuke, D. Pasko, A. Murray, T. Frayling, L. W. Harries, The splice site variant rs11078928 may be associated with a genotype-dependent alteration in expression of GSDMB transcripts. *BMC Genomics* **14**, 627 (2013).
- K. Miura, H. Mishima, M. Yasunami, M. Kaneuchi, M. Kitajima, S. Abe, A. Higashijima, N. Fuchi, S. Miura, K.-I. Yoshiura, H. Masuzaki, A significant association between rs8067378 at 17q12 and invasive cervical cancer originally identified by a genome-wide association study in Han Chinese is replicated in a Japanese population. *J. Hum. Genet.* **61**, 793–796 (2016).
- Y. Shi, L. Li, Z. Hu, S. Li, S. Wang, J. Liu, C. Wu, L. He, J. Zhou, Z. Li, T. Hu, Y. Chen, Y. Jia, S. Wang, L. Wu, X. Cheng, Z. Yang, R. Yang, X. Li, K. Huang, Q. Zhang, H. Zhou, F. Tang,

- Z. Chen, J. Shen, J. Jiang, H. Ding, H. Xing, S. Zhang, P. Qu, X. Song, Z. Lin, D. Deng, L. Xi, W. Lv, X. Han, G. Tao, L. Yan, Z. Han, Z. Li, X. Miao, S. Pan, Y. Shen, H. Wang, D. Liu, E. Gong, Z. Li, L. Zhou, X. Luan, C. Wang, Q. Song, S. Wu, H. Xu, J. Shen, F. Qiang, G. Ma, L. Liu, X. Chen, J. Liu, J. Wu, Y. Shen, Y. Wen, M. Chu, J. Yu, X. Hu, Y. Fan, H. He, Y. Jiang, Z. Lei, C. Liu, J. Chen, Y. Zhang, C. Yi, S. Chen, W. Li, D. Wang, Z. Wang, W. di, K. Shen, D. Lin, H. Shen, Y. Feng, X. Xie, D. Ma, A genome-wide association study identifies two new cervical cancer susceptibility loci at 4q12 and 17q12. *Nat. Genet.* **45**, 918–922 (2013).
39. Y. C. Yang, T.-Y. Chang, T.-C. Chen, W.-S. Lin, C.-L. Lin, Y.-J. Lee, Replication of results from a cervical cancer genome-wide association study in Taiwanese women. *Sci. Rep.* **8**, 15319 (2018).
40. S. Li, X. Li, S. Zhang, Y. Feng, T. Jia, M. Zhu, L. Fang, L. Gong, S. Dong, X. Kong, Z. Wang, L. Sun, Association between GSDMB gene polymorphism and cervical cancer in the Northeast Chinese Han population. *Front. Genet.* **13**, 860727 (2022).
41. S. S. Somanchi, K. J. McCulley, A. Somanchi, L. L. Chan, D. A. Lee, A novel method for assessment of natural killer cell cytotoxicity using image cytometry. *PLOS ONE* **10**, e0141074 (2015).
42. G. Suck, D. R. Branch, M. J. Smyth, R. G. Miller, J. Vergidis, S. Fahim, A. Keating, KHYG-1, a model for the study of enhanced natural killer cell cytotoxicity. *Exp. Hematol.* **33**, 1160–1171 (2005).
43. Q. Sun, J. Yang, G. Xing, Q. Sun, L. Zhang, F. He, Expression of GSDML associates with tumor progression in uterine cervix cancer. *Transl. Oncol.* **1**, 73–83 (2008).
44. G. Cardamone, E. Paraboschi, V. Rimoldi, S. Duga, G. Soldà, R. Asselta, The characterization of GSDMB splicing and backsplicing profiles identifies novel isoforms and a circular RNA that are dysregulated in multiple sclerosis. *Int. J. Mol. Sci.* **18**, 576 (2017).
45. D. Sarrio, A. Rojo-Sebastián, A. Teijo, M. Pérez-López, E. Díaz-Martín, L. Martínez, S. Morales, P. García-Sanz, J. Palacios, G. Moreno-Bueno, Gasdermin-B pro-tumor function in novel knock-in mouse models depends on the in vivo biological context. *Front. Cell Dev. Biol.* **10**, 813929 (2022).
46. Y. Zhang, J. Qian, C. Gu, Y. Yang, Alternative splicing and cancer: A systematic review. *Signal Transduct. Target. Ther.* **6**, 78 (2021).
47. T. H. Yang, Y.-H. Chiang, S.-C. Shiu, P.-H. Lin, Y.-C. Yang, K.-C. Tu, Y.-Y. Tseng, J. T. Tseng, W.-S. Wu, Cancer DEIso: An integrative analysis platform for investigating differentially

expressed gene-level and isoform-level human cancer markers. *Comput. Struct. Biotechnol. J.* **19**, 5149–5159 (2021).

Acknowledgments: We thank MD Anderson Sequencing and Microarray Facility (SMF) for Sanger sequencing. We thank X. Ma at Boston Children’s Hospital, S. Gu at MD Anderson Cancer Center, and J. Ruan at University of Connecticut Health Center for helpful discussion. **Funding:** This study was supported by the University of Texas Rising STARS Award and Elsa U. Pardee Research Grant to Z.Z.; National Institutes of Health grant R01CA240955 to J.L.; Howard Hughes Medical Institute funding, National Institutes of Health grant R01EB030015, and Rothenberg Innovation Initiative (RI2) at Caltech grant 25570017 to M.B.E.; National Institutes of Health grant R01AI139914 to H.W.; Ovarian Cancer Research Alliance Early Career Investigator Grant 649968 and Department of Defense grant W81XWH-18-PRCRP-CDA CA181455 to N.S.; National Institutes of Health grant R35GM133658, Komen Foundation grant CCR19609287, and the 2022–2023 program in Oncological Data and Computational Sciences sponsored by the Joint Center for Computational Oncology between the Oden Institute, MD Anderson, and TACC to S.S.Y.; postdoctoral fellowship from Jane Coffin Childs Memorial Fund for Medical Research to S.X.; and National Institutes of Health grant P30CA016672 to MD Anderson SMF. **Author contributions:** Q.K. and Z.Z. conceived the study. Z.Z., Q.K., and S.X. designed experiments and analyzed data. Q.K. performed most of the experiments with the assistance of Z.L., H.L., and X.T. S.X. performed structure analysis and modeling. X.P., N.S., and S.S.Y. performed bioinformatics analysis on tumor patient samples. K.Y. performed SNP genome-wide association studies analysis. J.L., X.L., S.X., M.B.E., and H.W. provided valuable editing and comments. Z.Z., Q.K., J.L., and S.X. wrote the manuscript. **Competing interests:** The authors declare that they have no competing interests. **Data and materials availability:** All data needed to evaluate the conclusions in the paper are present in the paper or the Supplementary Materials.

Submitted 15 December 2022
Accepted 6 April 2023
Published 28 April 2023
10.1126/sciimmunol.adg3196

Alternative splicing of *GSDMB* modulates killer lymphocyte–triggered pyroptosis

Qing Kong, Shiyu Xia, Xingxin Pan, Kaixiong Ye, Zhouyihan Li, Haoyan Li, Xiaoqiang Tang, Nidhi Sahni, S. Stephen Yi, Xing Liu, Hao Wu, Michael B. Elowitz, Judy Lieberman, and Zhibin Zhang

Sci. Immunol., **8** (82), eadg3196.
DOI: 10.1126/sciimmunol.adg3196

Cytotoxic pores require the right splice

Granzyme A (GzmA) is one of the cytotoxic granule proteins killer lymphocytes deploy to kill targeted tumor cells. Whereas GzmA-dependent cytotoxicity is reported to depend on pyroptosis activated by cleavage of gasdermin B (GSDMB), controversy has arisen over whether all splice variants of *GSDMB* can support formation of cytotoxic pores. Kong and Xia *et al.* assessed the ability of *GSDMB* isoforms to induce tumor cell death and found that only the *GSDMB3* and *GSDMB4* splice variants retaining exon 6 supported pyroptosis. The other *GSDMB* isoforms interfered with pyroptosis through a dominant negative mechanism. These findings better define the structural requirements for GzmA-dependent pyroptosis involved in antitumor immunity and reveal a mechanism by which some tumor cells can evade this killing pathway through modified splicing of *GSDMB* mRNA. —IRW

View the article online

<https://www.science.org/doi/10.1126/sciimmunol.adg3196>

Permissions

<https://www.science.org/help/reprints-and-permissions>

Use of this article is subject to the [Terms of service](#)

Science Immunology (ISSN) is published by the American Association for the Advancement of Science, 1200 New York Avenue NW, Washington, DC 20005. The title *Science Immunology* is a registered trademark of AAAS.

Copyright © 2023 The Authors, some rights reserved; exclusive licensee American Association for the Advancement of Science. No claim to original U.S. Government Works